Available online at www.sciencedirect.com

SciVerse ScienceDirect

Ceramics International 39 (2013) 6029–6033

CERAMICS INTERNATIONAL

www.elsevier.com/locate/ceramint

Structural and spectroscopic properties of Nd^{3+}:$Y_2Si_2O_7$ phosphors

Murat Erdem[a,*], Gönül Özen[b], Cumali Tav[a], Baldassare Di Bartolo[c]

[a]Marmara University, Department of Physics, Kadikoy, 34722, Istanbul, Turkey
[b]İstanbul Technical University, Physics Engineering, Maslak, 34469, Istanbul, Turkey
[c]Boston College, Department of Physics, Higgins 355, Chestnut Hill, MA 02467, USA

Received 22 October 2012; received in revised form 3 January 2013; accepted 8 January 2013
Available online 17 January 2013

Abstract

Phosphors of α-$Y_2Si_2O_7$ doped with Nd^{3+} ions were prepared using the sol–gel technique. Nano-sized crystalline phosphor powders were obtained by annealing the dried gels at 960 °C. The crystallization properties of the phosphor powders were determined from their XRD patterns. The α-$Y_2Si_2O_7$ phase was the only phase observed in all compositions. As the amount of amorphous SiO_2 in the composition was increased, the crystalline sizes and the widths of the size distribution curves were found to decrease from 17.8 nm to 10.6 nm and from 15.6 nm to 12.2 nm, respectively. The spectroscopic properties of the powders were studied by measuring the luminescence and the decay patterns of the $^4F_{3/2} \rightarrow {}^4I_{9/2}$ and $^4F_{3/2} \rightarrow {}^4I_{11/2}$ transitions between 50 K and 310 K. No appreciable effect of the crystallite sizes on the average lifetime of the $^4F_{3/2}$ level was observed at temperatures below 100 K. The effect of temperature, however, becomes relevant above 100 K as the size of α-$Y_2Si_2O_7$ nano-crystal becomes smaller.

Keywords: Nanophosphors; Sol–gel; Yittrium silicate; Life time

1. Introduction

The oxide phosphors have applications in high energy photo-luminescent (plasma panels), cathodoluminescent (field emission device) flat panel displays, solid state lasers, high energy phosphors and coherent time-domain optical memory applications [1–4]. These phosphors are composed of highly insulating host lattice compositions of yttrium oxide (Y_2O_3), yttrium orthosilicate (Y_2SiO_5), yttrium disilicate ($Y_2Si_2O_7$), and yttrium aluminaoxide ($Y_3Al_5O_{12}$) with fluorescence arising from the 3d→3d, 5d→4f or 4f→4f transitions in transition metal or rare earth ions.

High purity, compositionally uniform, single phase, small and uniform particle size phosphor powders are required for high resolution and high luminous efficiency in the new photonic device developments [5]. For instance, it has been shown that the smaller the phosphorus grain size, the higher the screen resolution, and the lower the screen loading for the flat panel displays [6]. In view of the nanotechnology, moreover, it should be pointed out that the selection of host lattices and active centers for such an optical material is important.

Fabrication of the complex host lattice compositions together with the controlled amounts of the activators (Cr^{3+}, Mn^{2+}, Ce^{3+}, Eu^{2+}, Eu^{3+}, Tb^{3+}, Nd^{3+}, Tm^{3+}) represent a challenge to the material synthesis community. The host lattice of yttrium disilicate may be doped, because it shows a high refractory property, chemical stability, etc. [7]. It has been shown that the structural phases due to its complex high temperature polymorphism are in the *y*, z, α, *β*, *γ*, and *δ* forms [8]. Yet, the main challenge is preparation of this composition as a single-phase material [9].

The insulating host materials doped with Nd^{3+} ions offer the possibility of UV, visible and IR emission channels according to a four-level scheme by direct excitation or by up conversion mechanism [10–12]. To our knowledge, only a few papers pertaining to the yttrium disilicate activated with rare earth (RE^{3+}: Ce^{3+}, Eu^{3+}, Tb^{3+}, Er^{3+}) exist [13–15], no

*Corresponding author. Tel.: +90 216 345 11 86/1118; fax: +90 216 347 87 83.
E-mail address: merdem@marmara.edu.tr (M. Erdem).

0272-8842/$ - see front matter © 2013 Elsevier Ltd and Techna Group S.r.l. All rights reserved.
http://dx.doi.org/10.1016/j.ceramint.2013.01.017

extensive studies of structural and luminescence properties of the yttrium disilicate activated with neodymium (Nd^{3+}) have been observed in the literature.

We present in this paper, a detailed investigation of the structural and luminescence properties of the single phase yttrium disilicate (α-$Y_2Si_2O_7$) activated with Nd^{3+} ions. In this study, choosing an appropriate mole ratio of SiO_2 to Y_2O_3 in the composition, a synthesis route and the annealing temperature, made it possible to obtain single phase (α-$Y_2Si_2O_7$) nanocrystalline phosphor powders with relatively uniform size distribution.

2. Experimental

Nanocrystalline yttrium silicate samples activated with Nd^{3+} were synthesized by using the sol–gel method. The neodymium acetate hydrate ($Nd(COOCH_3)_3 \cdot H_2O$), tetraethoxysilane (TEOS, $Si(OC_2H_5)_4$) and yttrium nitrate hexahydrate ($Y(NO_3)_3 \cdot 6H_2O$) were used to obtain three different compositions. For all the samples, SiO_2 and Y_2O_3 mole ratios taken as 1.5, 2.0 and 3.0, were labeled as YSN1, YSN2 and YSN3, respectively. The Nd^{3+} concentration in the YSN1, YSN2 and YSN3 samples before the heat treatment were determined to be 4.3×10^{19}, 4.7×10^{19}, 5.3×10^{19} cm^{-3}, respectively. Detailed description of the preparation process can be found in our earlier work [16]. The solutions at the final stage were poured into circular Petri dishes and left for 3 weeks at room temperature to obtain the transparent glass samples. The glass samples were then heat treated at 960 °C for 72 h to produce nanocrystalline α-$Y_2Si_2O_7$ powders.

The XRD images of both the glass samples and of those annealed at 960° for 72-h were taken by the model Shimadzu–XRD 6000 with the Cu-Kα source operated with the wavelength at $\lambda = 1.5418$ Å. Slit systems, step-size (0.02°), source voltage (40 kV) and current (30 mA) were kept constant during the scans that were conducted in θ–2θ coupled mode. The structural and morphological properties of the powders were also investigated by SEM images (JEOL JSM-6335F).

The average grain sizes of the powders were estimated from the X-ray patterns using the classical Scherrer equation which is based on the measurement of the full width at half maximum (FWHM) of the diffraction line. In addition to the grain sizes, the distribution of the grain sizes of the powders was also obtained using a method based on the two widths at 1/5 and 4/5 of the diffraction line maximum [17]. The latter method provides much more detailed information about the mean and the dispersion of the grain size distributions (GSD) than the Scherrer equation.

The luminescence spectra of the powders were measured using a diode laser (LDI-820) with the wavelength of 800 nm to excite a sample from the ground state ($^4I_{9/2}$) to the higher $^4F_{5/2}$ excited state. The luminescence from the powders was focused onto a Monochromator (Mc Pearson Model 2051) and detected by a PMT (Hamamatsu 7102) detector. For the decay measurements a Ti^{3+}: Sapphire Laser (Schwartz-SEO Electrooptics.Co.), 10 ns pulse duration, was used as an exciting source. The temporal evolution of the signal was obtained from a Tektronix Model 380 oscilloscope; the repetition rate was 10 Hz, and all the measurements were carried out at the temperature range from 50 K to 310 K obtained by a Janis Closed Cycle refrigerator.

3. Results and discussion

3.1. Morphology of phosphor powders

The crystalline phase formed was identified as the triclinic α-$Y_2Si_2O_7$ form [18] (space group $P\bar{1}$) by comparing the respective XRD patterns with the diffraction data of JCPDS card 38-0223. The X-ray patterns of all the powders are presented in Fig. 1 The intensity of the peaks corresponding to the α-$Y_2Si_2O_7$ crystalline phase increased with decreasing amount of amorphous SiO_2 in the powders.

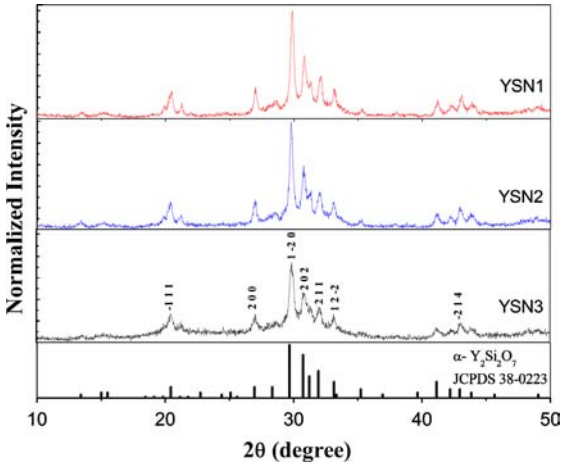

Fig. 1. XRD patterns of the YSN1, YSN2 and YSN3 phosphor powders.

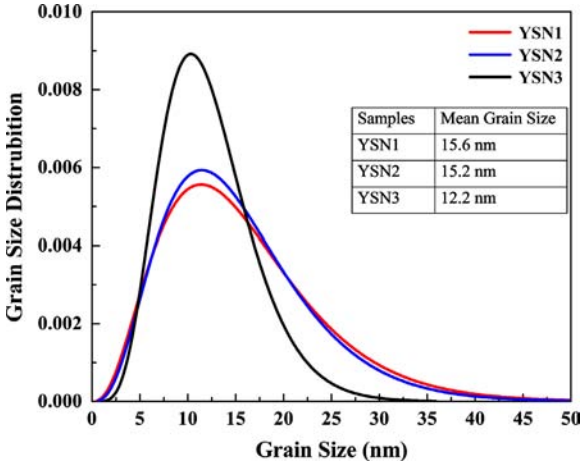

Fig. 2. Grain size distribution curves for the all phosphor powders.

Fig. 2 shows the grain size distribution (GSD) as function of the grain size. The average grain sizes of the YSN1, YSN2 and YSN3 powders were calculated to be about 22.9 nm, 21.5 nm and 14.2 nm from Scherrer equation, and to be 15.6 nm, 15.2 nm and 12.2 nm from the GSD curves, respectively. There is a discrepancy about the average grain sizes resulted from the two methods. This discrepancy might be due to the fact that the GSD is more sensitive than the Scherrer formula with respect to the widths of the XRD line maximum. It can also be seen from Fig. 2 that the GSD curves become more Gaussian while the width of the size distribution curves decreases from 17.8 nm to 10.6 nm for the 15.6 nm and 12.2 nm grain sizes, respectively. Moreover, the size of the α-$Y_2Si_2O_7$ nano-crystal obtained from both methods decreases as the amount of amorphous SiO_2 increases in the composition. This could be due to the fact that each Yttrium ion may be surrounded by more Silicon ions to form and/or to increase the size of the existing α-$Y_2Si_2O_7$ nano-crystals in the composition.

The α-$Y_2Si_2O_7$ crystalline phase observed in the SEM image of each powder is presented in Fig. 3a–c. The grains are nearly spherical, agglomerated, and with narrow size distribution in all the powders. The average diameter of the powders could not be determined from their respective SEM images because of the agglomeration.

3.2. Emission spectra and decay patterns

Figs. 4 and 5 present the emission spectra of the powders doped with Nd^{3+} ions in the wavelength range of 850–1150 nm at temperatures 50 K and 310 K. The insets in the figures correspond to the wavelength range of 1000–1150 nm. Each spectrum contains two transitions from the $^4F_{3/2}$ to $^4I_{11/2}$ and the ground level, ($^4I_{9/2}$) within the 4f shell of the Nd^{3+} ions. The emissions corresponding to the $^4F_{3/2}\rightarrow{}^4I_{9/2}$ and $^4F_{3/2}\rightarrow{}^4I_{11/2}$ transitions are centered about 892 nm and 1062 nm with FWHM values 58 nm and 28 nm, respectively. The J-manifolds of Nd^{3+} ions are split due to the low symmetry (C_1 or C_i) [19] of the α-$Y_2Si_2O_7$ cation sites; the spectral profile and the number of the Stark components are the same for all the powders. This behavior can be explained as due to the fact that the local symmetry of ligand ions surrounding the Nd^{3+} ions is the same for all samples because of the same crystalline phase. In addition, the emission intensity of the lines and bandwidth of the spectral profile for the $^4F_{3/2}\rightarrow{}^4I_{9/2}$, $^4F_{3/2}\rightarrow{}^4I_{11/2}$ transitions increase with increasing

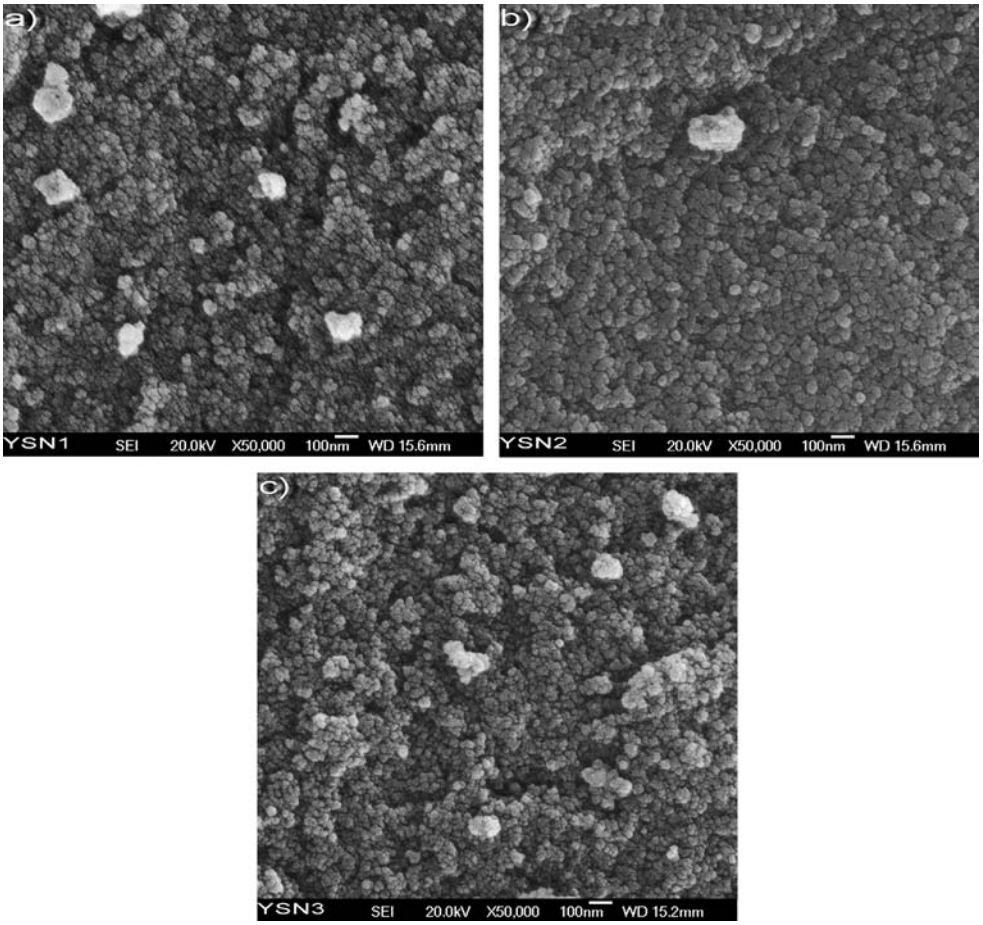

Fig. 3. SEM images of the (a) YSN1, (b) YSN2 and (c) YSN3 phosphor powders.

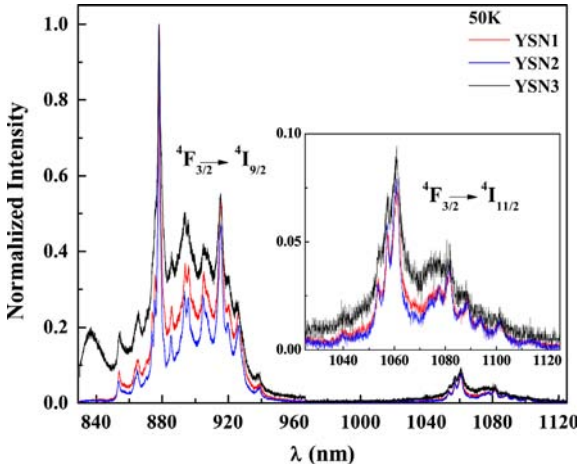

Fig. 4. Emission spectra of the phosphor powders for the $^4F_{3/2} \rightarrow {}^4I_{11/2}$, $^4I_{9/2}$ transition at 50 K.

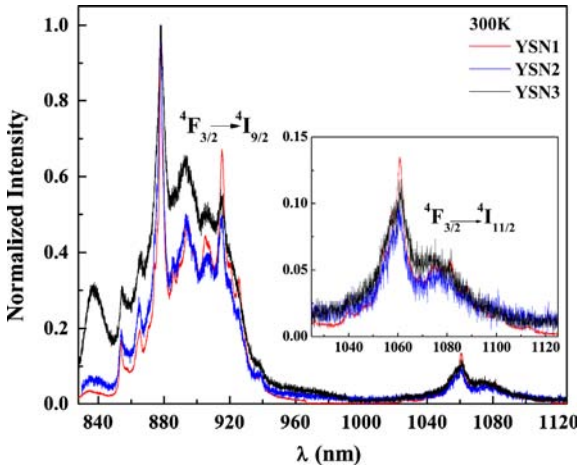

Fig. 5. Emission spectra of the phosphor powders for the $^4F_{3/2} \rightarrow {}^4I_{11/2}$, $^4I_{9/2}$ transition at 300 K.

temperature from 50 to 310 K. The change in intensity with temperature may be due to a change in the shape and the position of the absorption bands with temperature, a change that is particularly sensitive when the excitation is made by a sharp laser line.

The decay pattern of $^4F_{3/2}$ level was observed by monitoring the Nd^{3+} ions emission due to the $^4F_{3/2} \rightarrow {}^4I_{9/2}$ transition upon the excitation at 798 nm. The decay curves measured at various temperatures between 50 K and 310 K are illustrated in Fig. 6. The analyses of these curves lead us to conclusions about the effect of crystallite size and Nd^{3+} ion concentration. The decay patterns measured at 50 K are about the same for the powders that have different sizes ranging from 12.2 nm to 15.6 nm.

The average decay times of the $^4F_{3/2}$ emission as a function of temperature were determined from the decay patterns given in Fig. 6. The average lifetime was calculated according to the equation $\tau_{ave} = \int I/I_0 \, dt$ relation, where I_0 is the peak flourescence intensity. The lifetime of

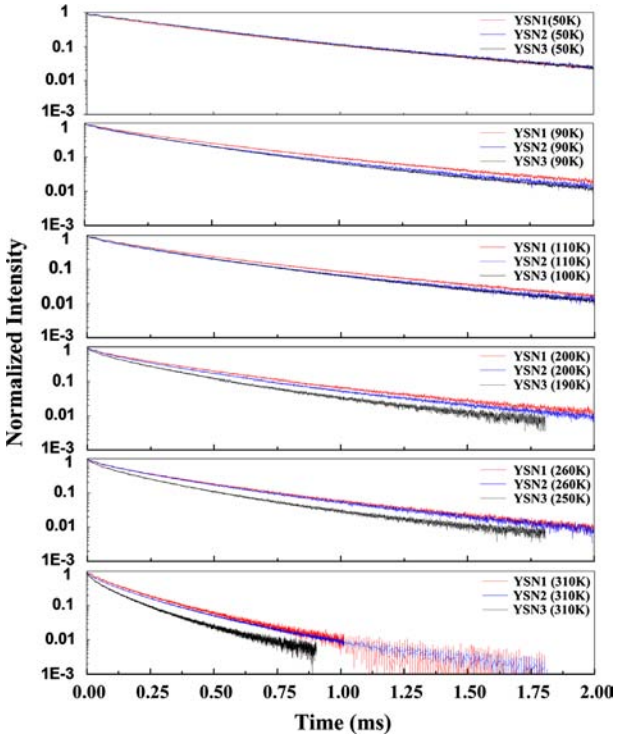

Fig. 6. Decay curves of the $^4F_{3/2}$ emission measured at various temperatures between 50 K and 310 K.

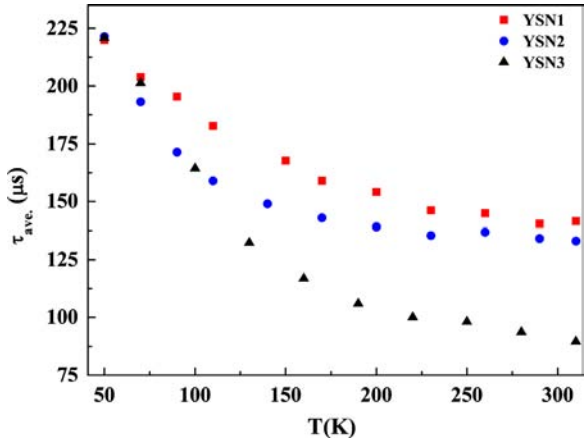

Fig. 7. Average decay times of the $^4F_{3/2}$ emission as a function of temperature.

the $^4F_{3/2}$ emission decreases as the concentration of the Nd^{3+} increases from 4.3×10^{19} to 5.3×10^{19} cm^{-3} in α-$Y_2Si_2O_7$ nano-crystalline powders when the grain sizes vary from 15.6 nm to 12.2 nm as seen in Fig. 7. The faster decay might be due to the effect of spatial confinement as well as of the Nd^{3+} concentration in the powders. Since the powder with the smallest grain size (YSN3) contains the highest Nd^{3+} concentration (5.3×10^{19} cm^{-3}), the effect of temperature on the decay patterns might be mainly due to the cross-relaxation processes between the Nd^{3+} ions. Hence, the decay patterns do not show direct

evidence about the effect of the grain sizes between 12.2 and 15.6 nm on the luminescence dynamics of the transitions initiating from the $^4F_{3/2}$ level of Nd^{3+} ions in α-$Y_2Si_2O_7$ nano-crystalline powders.

4. Conclusions

Using the sol–gel method, the structure and the luminescence properties of yttrium disilicate nano-phosphors activated with Nd^{3+} were synthesized and annealed at 960 °C for 72 h. Relative intensities of the peaks observed in the XRD patterns indicate that the volume fraction of the α-$Y_2Si_2O_7$ crystalline phase relative to the volume of the amorphous SiO_2 formed in the compositions increases. The method based on the measurements of the widths of the lines at the 1/5 and 4/5 of the maximum intensity of the diffraction lines results in more precise determination of the average grain sizes. This method also shows that the GSD curves become more Gaussian while the width of the size distribution curves decreases from 17.8 nm to 10.6 nm for the 15.6 nm and 12.2 nm grain sizes as the amount of amorphous SiO_2 increases in the composition.

The emission spectra and the decay patterns of the $^4F_{3/2} \rightarrow {}^4I_{9/2}$, $^4F_{3/2} \rightarrow {}^4I_{11/2}$ transitions do not show a clear evidence for the crystalline size effect at all temperatures from 50 K to 310 K. However, the effect of the Nd^{3+} concentration and the temperature on the decay patterns and the average lifetime of the $^4F_{3/2}$ level which serves as the upper level for the 1.06 μm laser transition were observed. The average lifetime of the $^4F_{3/2}$ level was measured to be the same with an average value 221 μs at 50 K while it was determined to be 141.5 μs, 133.1 μs and 88.5 μs at 310 K for the 15.6 nm, 15.2 nm and 12.2 nm grain sizes, respectively.

Acknowledgment

This study was financially supported by the Science Institute of Marmara University with the project number FEN-C-DRP-090409-007.

References

[1] M. Jacquement, F. Balembois, S. Chenais, S. Druon, P. Georges, R. Gaume, B. Ferrand, First diode-pumped Yb-doped solid-state laser continuously tunable between 1000 and 1010 nm, Applied Physics B 78 (2004) 13–18.

[2] P. Zhou, X. Yu, L. Yang, S. Yang, W. Gao, Synthesis of $Y_2Si_2O_7$: Eu nanocrystal and its optical properties, Journal of Luminescence 124 (2007) 241–244.

[3] D. Hreniak, P. Gluchowski, W. Strek, M. Bettinelli, A. Kozlowska, M. Kozlowski, Preparation and upconversion properties of Er^{3+}, Yb^{3+}:$Y_2Si_2O_7$ nanocrystallites embedded in PVA polymer nanocomposites, Materials Science 24 (2006) 405–413.

[4] M. Mitsunaga, R. Yano, N. Uesugi, Time-and frequency-domain hybrid optical memory: 1.6-kbit data storage in Eu^{3+}:Y_2SiO_5, Optics letters 16 (1991) 1890–1892.

[5] B.M. Tissue, Synthesis and Luminescence of Lanthanide Ions in Nanoscale Insulating Hosts, Chemistry of Materials 10 (1998) 2837–2845.

[6] E.J. Boszea, G.A. Hirataa,b, L.E. Shea-Rohwerc, J. McKittrick, Improving the efficiencyof a blue-emitting phosphor by an energy transfer from Gd^{3+} to Ce^{3+}, Journal of Luminescence 104 (2003) 47–54.

[7] M.D. Dolan, B. Harlan, J.S. White, M. Hall, S.T. Misture, S.C. Bancheri, B. Bewlay, Structures and anisotropic thermal expansion of the α, β, γ, and δ polymorphs of $Y_2Si_2O_7$ Phosphor, Powder Diffraction 23 (2008) 20–25.

[8] J. Felsche, The crystal chemistry of rare-earth silicates, Structure and Bonding 13 (1973) 99–197.

[9] L. Marciniak, D. Hreniak, A. Dobrowolska, E. Zych, Size-dependent luminescence in $Y_2Si_2O_7$ nanoparticles doped with Ce^{3+} ions, Applied Physics A 99 (2010) 871–877.

[10] R.M. Macfarlane, F. Tong, A.J. Silversmith, W. Lenth, Violet cw neodymium upconversion laser, Applied Physics Letters 52 (1988) 1300–1303.

[11] M.J. Weber, Science and technology of laser glass, Journal of Non-Crystalline Solids 123 (1990) 208–222.

[12] D.S. Funk, J.M. Carlson, J.G. Eden, Ultraviolet (381 nm) room temperature laser neodymium-doped fluorozirconate fibre, Electronics Letters 30 (1994) 1859–1860.

[13] N. Karar, H. Chander, Luminescence properties of cerium doped nanocrystalline yttrium silicate, Journal of Physics D: Applied Physics 38 (2005) 3580–3583.

[14] J. Sokolnicki, Rare earths (Ce,Eu,Tb) doped Y2Si2O7 phosphors forwhite LED, Journal of Luminescence 134 (2012) 600–606.

[15] N. Taghavinia, G. Leronda, H. Makino, T. Yao, Europium-doped yttrium silicate nanoparticles embedded in a porous SiO_2 matrix, Nanotechnology 15 (2004) 1549–1553.

[16] M. Erdem, G. Özen, C. Tav, Crystallization behaviour of neodymium doped yttrium silicate nanophosphors, Journal of the European Ceramic Society 31 (2011) 2629–2631.

[17] R. Pielaszek, FW1/5-4/5M method for determination of the grain size distribution from phosphor powder diffraction line profile, Journal of Alloys and Compounds 382 (2004) 128–132.

[18] A.I. Becerro, A. Escudero, Revision of the crystallographic data of polymorphic $Y_2Si_2O_7$ and Y_2SiO_5 compounds, Phase Transitions 77 (2004) 1093–1102.

[19] Kaminskii Alexander A, Crystalline Lasers: Physical Processes and Operating Schemes, CRC Press, New York, 1996, pp. 95–100.